Mon. Not. R. Astron. Soc. **325,** 665–675 (2001)

The milliJansky 12-μm population: first follow-up

D. L. Clements,[1,2★] F.-X. Desert[3] and A. Franceschini[4]

[1]*Department of Physics and Astronomy, Cardiff University, PO Box 913, Cardiff, CF24 3YB*
[2]*Institut d'Astrophysique Spatiale, Bâtiment 121, Universite Paris XI, F-91405 ORSAY CEDEX, France*
[3]*Observatoire de Grenoble, BP 53, 414 Rue de la Piscine, 38041 Grenoble Cedex 9, France*
[4]*Osservatorio di Padova, Vicolo Osservatorio, 5, 35122 Padova, Italy*

Accepted 2001 February 26. Received 2001 February 20; in original form 2000 September 11

ABSTRACT

We present the first results of our follow-up programme of optical imaging and spectroscopy of a deep 12-μm survey conducted with the *ISO* satellite. We find that the objects are typically of fairly low redshift ($z \sim 0.1$–0.2), but with a tail that extends to high redshifts. The highest redshift object is a previously unknown quasar at $z = 1.2$. The sample of objects for which spectroscopy has been obtained forms a complete subsample of the original survey with an *R*-band magnitude limit of 19.6. We are thus able to use *accessible volume* methods to determine the luminosity function. We find that the luminosity function is close to the low-redshift 12-μm luminosity function determined by *IRAS*, but with a possible excess at the highest luminosities, which also correspond to the highest redshifts. This excess is compatible with the rapid luminosity evolution of $L \propto (1 + z)^{4.5}$ claimed by Xu and suggested by Elbaz et al. on the basis of number counts. These conclusions remain tentative because of small number statistics at the highest redshifts.

Almost all of the galaxies in this survey are emission line objects. We use the spectra to determine emission line diagnostics for the underlying ionization source. We find that the majority of objects have H II region-like spectra (roughly 2/3) but there is a significant fraction (about 1/3) that contain an active galactic nucleus (AGN). This confirms suspicions that deep mid-IR surveys will be a powerful way to find obscured AGN. Part of the survey area has been imaged deeply by the INT Wide Field Camera. Nearly all 12-μm sources in this area, down to the 3σ sensitivity limit of the original *ISO* survey, have good optical identifications, the faintest being at $R = 23$. The prospects are thus good for obtaining complete spectroscopy for this sample. With such data we should be able to make a clear measurement of the evolution rate of this population and determine the role of obscured AGN in the mid-infrared.

Key words: galaxies: active – galaxies: evolution – galaxies: starburst – infrared: galaxies.

1 INTRODUCTION

The *ISO* satellite (Kessler et al. 1996) has vastly increased our observational capabilities in the mid- and far-infrared (mid- and far-IR), and has ushered in a new series of deep cosmological surveys at these wavelengths (e.g. Oliver et al. 2000; Elbaz et al. 1999; Kawara et al. 1998; Puget et al. 1999; Clements et al. 1999). In the mid-IR these surveys reach flux limits more than 100 times fainter than our previous best surveys with *IRAS* (Hacking, Houck & Condon 1987), whilst also attaining substantially improved spatial resolution. They thus represent an important new tool for observational cosmology. They are especially important since there is increasing evidence that much of the star formation activity in the universe is obscured by dust, which re-radiates the energy absorbed at optical and UV wavelengths into the mid- and far-IR. While the discovery of luminous and ultraluminous infrared galaxies (LIGs and ULIRGs) in the local universe by *IRAS* was the first hint of the potential importance of obscured emission (see e.g. Saunders & Mirabel 1996, and references therein), it wasn't until the discovery of the cosmic infrared background (CIB) (Puget et al. 1996) and large numbers of discrete sources in SCUBA submillimetre surveys (e.g. Eales et al. 1999) and ISOPHOT far-IR surveys (e.g. Puget et al. 1999) that the cosmological significance became clear. It now seems that such obscured objects might contribute up to 2/3 of the integrated emission in the universe (Gispert, Lagache & Puget 2000) and thus might be the

★E-mail: d.clements@astro.cf.ac.uk

sites for the majority of star formation. Alternatively, a significant number of the obscured sources might be powered by active nuclei, and thus the sources uncovered by mid- and far-IR surveys might tell us much about the formation of quasars, and hence about the cosmic X-ray background (Almaini, Lawrence & Boyle 1999).

While much of the emission from obscured sources will be emitted in the far-IR, at wavelengths $>50\,\mu$m, there are substantial advantages in pursuing surveys in the mid-IR, at wavelengths between 10 and 20 μm. These are primarily to do with the limitations of the current generation of instruments. As *ISO* had only a 60-cm mirror, the angular resolution attainable at long, far-IR wavelengths is quite poor, leading to problems with confusion and with identifications for follow-up surveys. These difficulties are largely avoided in the mid-IR. The mid-IR region was also the most sensitive on *ISO*, with improvements up to 100 times over *IRAS*, while the far-IR typically only reached 10 times greater depths, partly as a result of confusion noise (Puget et al. 1999). Despite operating at shorter wavelengths, the mid-IR is still capable of detecting obscured star formation regions. For example, the Antennae galaxy has optically prominent galactic nuclei, but mid-IR images, obtained with ISOCAM (Mirabel et al. 1998), show that the bulk of the star formation resides between these nuclei, in a region of high obscuration. The peak of the mid-IR flux also coincides with the peak of both the 850-μm emission, as seen by SCUBA, and the peak of the molecular emission, as revealed by CO observations (Haas et al. 2000, and papers in Hughes & Lowenthal 2000).

Mid-IR observations, however, do have some problems. These are principally the result of the complex spectral energy distributions (SEDs) in the mid-IR band. For starburst galaxies, which are likely to be the majority of the objects found in a deep mid-IR survey, the SED is dominated by the so-called unidentified infrared bands (UIBs), which produce prominent broad features at wavelengths of 6.2, 7.7, 8.6, 11.3 and 12.7 μm, and can vary in strength from object to object. Furthermore, there is also the possibility of emission and absorption line contributions, the strongest of which will be the Si absorption feature at 9.7 μm. The effect of these features on cosmological surveys in the mid-IR has been extensively studied by Xu et al. (1998). They find that the effects of these features will be more pronounced the narrower the observational passband. While most deep cosmological mid-IR surveys have been conducted in the 15-μm band, the present work uses the broader 12-μm filter. The Xu et al. modelling clearly shows that this filter will be less susceptible to the effects of the complex SED.

The current results of deep mid-IR surveys with *ISO* are summarized by Elbaz et al. (1999; but see also Serjeant et al. 1997; Clements et al. 1999; Oliver et al. 2000; Serjeant et al. 2000). Substantial evolution in the number counts, beyond no-evolution extrapolations from the local population, has been found (e.g. Elbaz et al. 1999). The meaning of these counts, though, is still unclear. Elbaz et al. (1998), for example, claim that a new population of objects becomes significant at flux levels of <1 mJy at 15 μm, producing a distinct bump in the number counts. They suggest that this is a new population of objects at $z < 1.5$ contributing a substantial amount of the star formation history of the universe. Meanwhile, Xu (2000) suggests that a combination of simple luminosity evolution at a rate of $L \propto (1+z)^{4.5}$ combined with the colour effects of the UIB features can produce the jump in number counts seen in the data. It is not possible to decide between these possibilities using the existing number-count data. The only way to determine the true nature and significance of the sources uncovered by deep mid-IR surveys is to determine their redshifts, and thus to explicitly measure their luminosity function and evolution. Various models of this population can then be explicitly tested. We cannot yet directly obtain redshifts for mid-IR sources in the waveband of detection, but must instead use ground-based optical and/or near-IR observations. Identifications, and spectra, at these complementary wavelengths must thus be obtained.

We here report the first results from identification and redshift measurements for a deep 12-μm *ISO* survey (Clements et al. 1999) conducted using the ISOCAM instrument (Cesarsky et al. 1996) on the *ISO* satellite. The survey covers a total area of 0.1 square degrees made up of four separate sub-regions separated by several degrees, and reaches a 3σ flux limit of $\sim$300 μJy. A total of 148 sources were detected above the 3σ limit, though a number of these may still be fragments of brighter sources. Where optical identifications in the US Naval Observatory Catalogue (USNO-A) are available, we can achieve star–galaxy separation using an optical–IR colour–colour method. This relies on the stellar spectra approximating a single temperature blackbody, while the galaxies are assumed to have a substantial infrared excess. Very few of the galaxies found in the survey were previously known. Only one object, which was detected by *IRAS*, had a measured redshift. A full description of this 12-μm survey is given in Clements et al. (1999) (hereafter Paper I). The goal of the present paper is to present the first results of the follow-up programme aimed at this survey.

The rest of this paper is organized as follows. In the next section we describe the sample of objects observed, and after that the observations themselves. The results of the spectroscopy are then discussed, followed by brief comments on the identification of 12-μm sources in two previously blank fields. Discussion of the luminosity function of the 12-μm sources and then emission line diagnostics for their power sources follows. We then discuss the nature and significance of this population before drawing our conclusions. An H_0 of 75 km s^{-1} Mpc^{-1} and $q_0 = 0.5$ are assumed throughout.

2 THE SAMPLE

The target list for the spectroscopic follow-up was constructed from the list of $>5\sigma$ non-stellar sources given in Paper I. From these we then selected those objects with an optical identification (ID) brighter than $R = 19.6$ mag, as cross-identified in the USNO-A catalogue. This provides a list of 25 objects. (The object F3_15 was found to be a star in Paper I on the basis of its optical–IR colours. This stellar identification was inadvertently missed from table 2 in that paper, but was included for the analysis work in that paper. It is thus not part of the basis sample in the current work.)

As part of the INT Wide Field Survey (INT WFS; McMahon et al. 2000) and the UKIRT mini-survey (Davies et al., private communication), much of Field 1 of Paper I was observed in the optical–near-IR, providing *UBVRIJK* images and photometry. The identifications and fluxes from USNO-A can thus be checked and are found to be broadly correct. The deeper optical data also allows us to go fainter in our identifications of *ISO* sources in Field 1. We find that all of the $>5\sigma$ *ISO* sources are identified in this field (the faintest is F1_44, which is identified with an *R*-band object with $R = 23.15$). We also attempt to obtain identifications for fainter $3-5\sigma$ significance *ISO* sources using the new optical data. We find good identifications by eye for all except three *ISO* sources $>3\sigma$ within the area covered by the INT WFS image. These three

Table 1. Properties of the 12-μm sources: the source name is given by catalogue number in appropriate field (F1 to F4), as in Paper I. Objects already known to be stars from Paper I have been excluded. *R*-band magnitudes in Field 1 come from the INT WFC survey data, others come from the USNO-A catalogue. Signal-to-noise ratio for the 12-μm detection can be estimated from the flux error. Bolometric luminosity is calculated using the conversion from 12-μm to bolometric luminosity determined by Spinoglio et al. (1993) and the classifications from emission line diagnostics. A 'mixed' class object is treated conservatively as being an AGN. Where emission line diagnostics are unavailable the object is treated as a starburst.

Object	RA (^{h} ^{m} ^{s})	Dec (2000) ($^{\circ}$ $'$ $''$)	F_{12} (2000)	R_{mag} (μJy)	Redshift (z)	Log (12-μm Luminosity) ($L_{\odot}$)	Log (Bolometric Luminosity) ($L_{\odot}$)
F1_0	03 05 36.2	−09 31 21.6	12147 ± 200	17.1	0.113	10.1	11.2
F1_3	03 05 15.1	−09 31 17.6	3835 ± 99	18.6	0.191	10.1	11.2
F1_4	03 05 05.3	−09 32 07.7	2150 ± 185	19.5	0.249	10.1	11.2
F1_5[a]	03 05 24.5	−09 35 50.7	1046 ± 102	20.2	0.478	10.6	11.7
F1_7	03 05 39.5	−09 31 25.7	968 ± 241	19.1	0.114	9.0	10.1
F1_9	03 05 35.9	−09 31 43.8	3732 ± 142	18.6	0.115	9.6	10.7
F1_10	03 05 06.1	−09 32 41.5	1903 ± 185	17.9	0.113	9.3	10.5
F1_11	03 05 14.9	−09 31 03.8	1324 ± 113	18.9	0.290	10.1	10.8
F1_12	03 05 28.4	−09 35 17.5	842 ± 92	16.9	0.461	10.4	11.1
F1_18	03 05 36.3	−09 31 32.2	2190 ± 171	18.5[b]	0.113	9.3	10.5
F1_30	03 05 30.7	−09 33 13.4	636 ± 88	18.8	0.138	9.0	9.7
F1_34	03 05 39.0	−09 38 32.2	563 ± 115	18.3	0.098	8.6	9.3
F1_48	03 05 11.0	−09 33 10.0	605 ± 119	19.1	0.120	8.8	9.9
F2_0	03 01 06.1	−10 44 27.5	10479 ± 260	13.0	0.032	8.8	9.9
F2_3	03 00 37.3	−10 42 51.0	2385 ± 100	18.8	0.171	9.8	10.5
F2_24	03 00 35.4	−10 43 22.3	814 ± 118	18.5	0.119	9.0	9.7
F2_80	03 00 39.5	−10 39 43.4	522 ± 89	19.5	0.093	8.5	9.6
F3_3	03 10 00.9	−08 39 39.2	1760 ± 95	14.6	M star		
F3_4	03 10 09.1	−08 38 57.2	1682 ± 105	17.6	0.107	9.1	10.2
F3_5	03 09 44.7	−08 32 55.6	1374 ± 108	17.0	0.132	9.3	10.4
F3_34	03 09 46.1	−08 32 44.0	639 ± 105	17.9	0.576[c]	10.6	
F4_1	03 04 03.4	−10 01 18.0	3670 ± 149	17.9	0.175	10.0	11.1
F4_3	03 03 55.2	−09 56 59.9	3207 ± 84	16.6	0.171	9.9	10.6
F4_5	03 03 47.3	−09 59 18.2	2481 ± 215	19.0	0.383	10.7	11.4
F4_6	03 04 06.3	−09 53 47.6	3051 ± 197	16.6	0.214	10.1	11.2
F4_9	03 03 56.8	−09 57 31.3	1234 ± 95	17.6	0.171	9.5	10.6
F4_12	03 03 54.7	−09 58 45.6	933 ± 106	19.1	1.2	12.0	12.7

Notes. [a]Additional object below nominal *R*-band magnitude limit. [b]Source outside region covered by INT WFC survey, *R*-band magnitude from USNO-A catalogue. [c]Insecure redshift based on absorption feature. All other redshifts based on emission lines.

unidentified sources are all of low signal-to-noise ratios, (3.5, 3.0 and 3.2 σ) and so might be residual noise spikes or cosmic hits that have managed to escape our ISOCAM reduction. The reliability of the source detection, discussed in Paper I, with only 4 per cent of initially detected sources being rejected as spurious cosmic hits, suggests that these may be real sources. We thus conclude that the optical imaging, to about $R = 23.5$, which identifies 26 *ISO* sources and fails on these three, has a maximum identification incompleteness of ∼11 per cent. This bodes well for obtaining complete identifications for the $3-5\sigma$ sources in the other three fields with deeper optical imaging, which has now been obtained (Clements et al., in preparation).

The basic properties of the sources observed in this project are given in Table 1.

3 OBSERVATIONS

Most of the observations were carried out at the ESO 3.6-m telescope at La Silla from 1999 November 13 to 15. We used the EFOSC2 instrument. This provides both imaging and long slit spectroscopic capabilities, using filters and grisms (Patat 1999). The detector is a 2060 × 2060 thinned Loral CCD which has good sensitivity throughout the optical spectrum. The pixel scale is 0.157 arcsec pixel^{-1}. Most of the spectra discussed here were taken using a 2-arcsec wide slit, though a few used a 1-arcsec slit, and Grism 12, which covers the spectral region from ∼6000 to 10 000 Å at 2.12 Å pixel^{-1} dispersion. A few objects were also observed in the blue using Grism 11 which covers ∼3400 to 7500 Å at the same resolution. Wavelength calibration was achieved using a He–Ar arc lamp attached to the spectrograph, while flat fielding used a dome flat. The contribution of sky lines to the spectra was calculated by fitting and subtracting a cubic spline function to the spatial direction for each detector row in the dispersion direction. Standard *IRAF* tasks were used for these procedures. The CCD response function was calibrated out of the spectra using observations of the spectroscopic standard stars LTT9239 and LTT1020. Spectroscopy integration times ranged from 900 to 1800 s. Typical observing conditions were for seeing between 1 and 2 arcsec, and with reasonable transparency. The conditions, however, were not sufficiently stable to be photometric.

Two objects, F1_0 and F2_0, were observed on a previous run, from 1997 December 24 to 25, which was severely affected by poor conditions and equipment problems. This was also conducted at the ESO 3.6-m telescope using EFOSC2. The observational setup was broadly similar, though a different grism, Grism 1, was used. This covers ∼ 3200–10000Å at 6.3 Å pixel^{-1}. The observations and data reduction for these objects followed the same scheme described above. The reduced resolution, however, means that these observations cannot be used for emission line diagnostics.

In addition to the spectroscopic observations, *R*-band imaging was also obtained for two objects during the 1999 run. These were F4_2 and F4_11, chosen to be bright 12-μm sources, with strong detections in the ISOCAM observations, but without a bright ($R < 19.6$) optical identification. The images were taken as a series of four separate 200-s integrations, each shifted by −30 arcsec in both Dec. and RA. The images were flat-fielded using an imaging

dome flat, and then median-stacked with the appropriate shifts taken into account. Residuals left after the dome flat were them corrected be median stacking the images for both objects with each other without the shifts corrected, to provide a secondary, sky flat image.

4 RESULTS

4.1 Spectroscopic results

The reduced spectra were all visually inspected and initial classifications, such as stars, emission-line galaxies and, in one case, a possible absorption-line galaxy, were made on this basis. The vast majority of objects turned out to be emission-line galaxies. These spectra were further analysed to extract redshifts, determine emission-line strengths, and to search for broad emission lines. Redshifts and derived properties are summarized in Table 2. The following method was used to extract spectral properties. First, the brightest pixel in a given wavelength range is assumed to be Hα. Then a composite spectrum, including a background flux that is constant with respect to wavelength, Hα, [N II] and [S II] emission lines, is matched to the spectrum. The lines are assumed to have Gaussian shapes, with [N II] and [S II] lines having the same width but different widths from Hα. The strengths of the Hα, [N II] and [S II] lines are allowed to vary, but the ratios of the [S II] and [N II] doublets are fixed at their physical values (Osterbrock 1989). The assumed redshift is also allowed to vary. The χ^2 between the model and the observed spectrum is minimized using a downhill simplex method (AMOEBA in IDL). Where a broad line is suspected, an additional model component consisting of an extra Hα with larger initial Gaussian width is added to see if the χ^2 is significantly reduced. This is found to be the case in only one object. The results of these fits are given in Table 2, as are the results of the spectroscopy more generally. Spectra are shown in Fig. 1 and, for the one quasar in the sample, F4_12, in Fig. 2.

Given the redshifts, we then calculate the 12-μm luminosities of the objects in the usual manner. We include a *K*-correction to account for the effects of the complex SED in the mid-infrared. The *K*-correction adopted is a simple linear fit to the models of Xu et al. (1998). Over the redshift range of interest (0–1.2) the Xu *K*-corrections can be approximated as $K = 1.7z$, using the definition of *K*-correction from Xu et al. (1998). However, this is the mean *K*-correction and does not take into account the effects of SED differences from one object to another. These differences, however, are smaller in the *ISO* 12-μm band than in any of the other *ISO* filters used for deep ISOCAM surveys (Xu et al. 1998). The uncertainties produced by this scatter should be less than $\sim$0.2 mag, and thus should not have a major effect on the luminosity function we derive from these luminosities.

4.1.1 *Notes on specific objects*

(i) **F3_3**. This object was classified as a galaxy based on its

Table 2. Emission-line equivalent widths (EW) and derived classifications for objects where emission-line classifications are possible. H II indicates an H II region-like spectrum, and thus an object likely to be powered by a starburst. Sy1 and Sy2 indicate a Seyfert 1 (ie. broad line) and Seyfert 2 spectrum respectively, and thus the presence of, and probable powering by, an AGN. M indicates a spectrum that may be a mixture of H II and Sy2, or may be a LINER – the current limited set of emission lines cannot discriminate between these possibilities. '*A* band' indicates that the relevant lines are affected by atmospheric absorption by the *A* band, leading to uncertain equivalent widths. In most of these cases classification is not possible. '?' indicates that the current measurements or limits to equivalent widths do not permit classification. In some cases there are second classifications indicated by *. These are classifications which include the Hβ and [O III] fluxes when they are available. In the case of 'M' and '?' classifications these later, more complete, classifications are adopted.

Object	Redshift	Hα EW	[N II] EW	[S II] EW	Hα (broad)	Class
F1_3	0.191	104.6	60.7	26.4		H II
F1_4	0.249	41.5	21.0	15.0		H II
F1_5	0.478	50.3	33.4	<48		?, H II*
F1_7	0.114	14.7	4.9	1.8		H II
F1_9	0.115	26.7	11.1	10.0		H II
F1_10	0.113	17.0	6.4	4.3		H II
F1_11	0.290	21.7	35.9	<3.0		M, H II*
F1_12	0.461	54.9	53.0	30.7		Sy2, Sy2*
F1_18	0.113	79.1	50.1	24.9		H II
F1_30	0.138	28.1	20.1	2.7		M
F1_34	0.098	9.1	13.6	3.4	26.4	Sy1
F1_48	0.120	61.3	26.7	21.2		H II
F2_3	0.171	13.25	13.3	8.8		Sy2
F2_24	0.119	17.3	20.2	17.2		Sy2
F2_80	0.093	56.9	17.1	18.1		H II
F3_4	0.107	49.6	21.0	13.2		H II
F3_5	0.132	21.2	10.9	*A* band		H II
F4_1	0.175	35.0	20.9	10.3		H II
F4_3	0.171	14.1	11.9	5.7		Sy2
F4_5	0.383	46.7	44.8	9.5		M, Sy2*
F4_6	0.214	11.3	6.6	1.8		H II
F4_9	0.171	*A* band	*A* band			
F4_12	1.2					Sy1

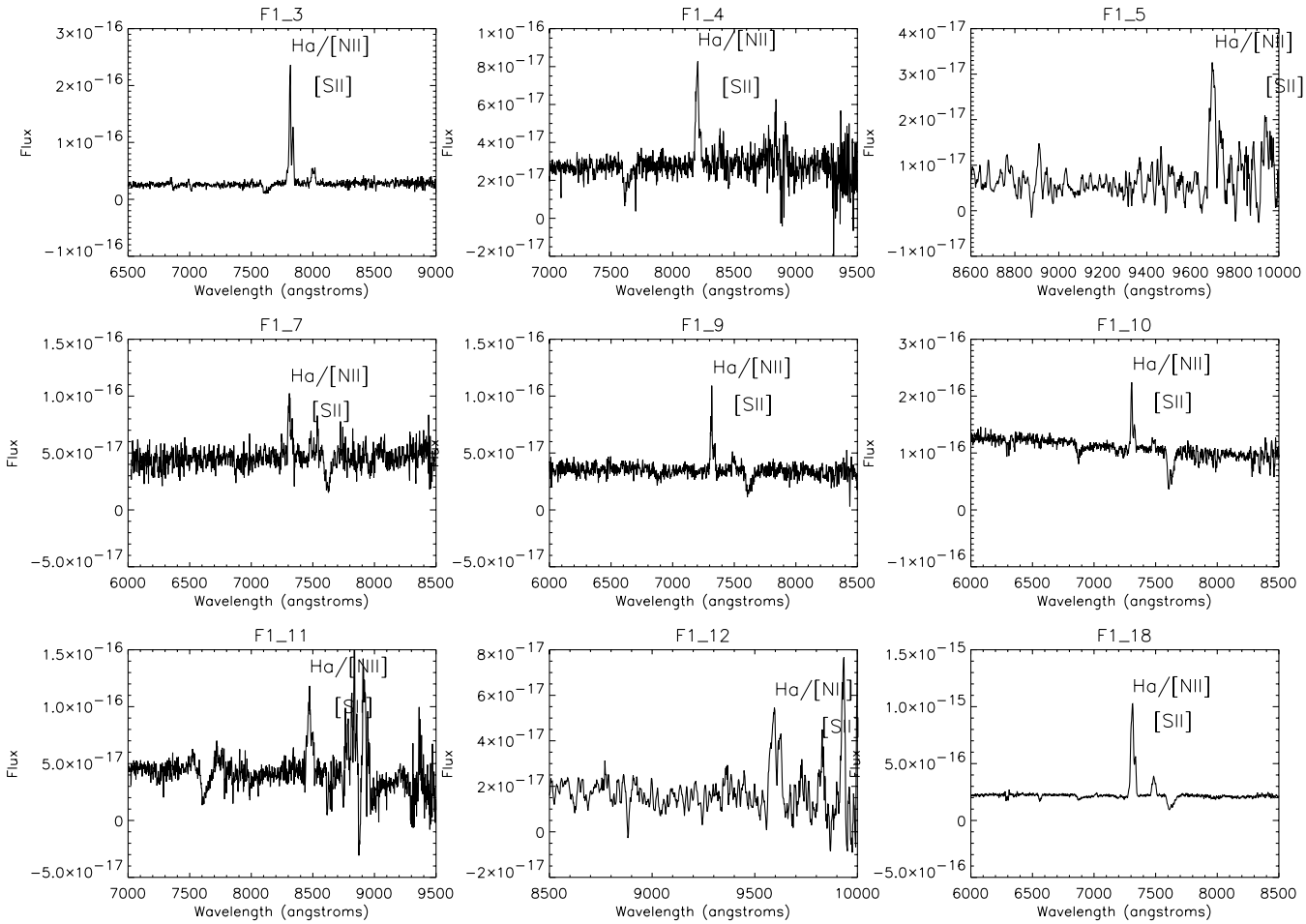

Figure 1. Observed spectra: spectra for the galaxies observed in this programme. The locations of important features typically Hα and S II are indicated and the wavelength range shown is chosen to highlight these features. Spectrophotometric calibration is not fully calibrated, so the flux values are indicative only. The objects F1_0 and F2_0 were observed in poor conditions on an earlier observing run. These two spectra are not flux calibrated merely divided through by a standard star so the apparently blue continuum slope is not real.

location on the $B{-}R{-}F_{12}$ colour–colour diagram (Paper I). However, spectroscopy clearly shows that the object is an M star. The previous misclassification is probably a result of the large molecular absorption bands in the M-star spectrum suppressing optical emission below what would be expected from a simple blackbody spectrum.

(ii) **F1_34**. The Hα emission line in this object appears to be broad: $\sim$1000 km s^{-1} (cf. 400 km s^{-1} for the other, narrow lines), indicating the likely presence of a Seyfert 1 (Sy1) active nucleus.

(iii) **F4_12**. At $z = 1.2$ this is the highest redshift object in the sample. It is also the only object in the sample that is characterized by a clear broad-line spectrum, containing emission lines of Mg II and Al II/C III. There also appears to be a broad emission feature to the blue of Mg II which could be due to Fe II. The Mg II full width at half-maximum (FWHM) is found to be 4300 km s^{-1} (observed frame). The spectrum is shown in Fig. 2.

5 BLANK FIELDS

10 sources from Paper I are as yet optically unidentified. Thus, at the same time as our optical spectroscopy, we also obtained moderately deep images for two 12 μm optical blank-field sources, F4_11 and F4_2. These are shown in Fig. 3. In both cases we find plausible faint optical identifications within 7 arcsec of the *ISO* source position. In the case of F4_11, the identification is isolated and unambiguous. In the case of F4_2, however, there would appear to be a group of similar faint objects close to the primary identification. There is thus the potential that the *ISO* source may be a combination of two, possibly interacting, objects, or that the identification might be one of the other optical sources in the field.

We can obtain an estimate for their magnitude by comparison with magnitudes of known objects imaged at the same time. We find that F4_11 has $R \sim 20$ and F4_2 has $R \sim 22$. These results are consistent with the results from the INT WF survey data discussed earlier.

With identifications obtained for these two sources, there remain eight sources with *ISO* detections $>5\sigma$ that still lack optical identifications. As these are the objects with the highest 12-μm to optical ratios, they are clearly interesting targets. Their optical faintness suggests that they are at high redshifts, and they are thus likely to be highly luminous. Further observations will be proposed to obtain identifications and redshifts for these, and fainter *ISO* sources.

6 THE LUMINOSITY FUNCTION

The data presented in this paper provides redshift information for a

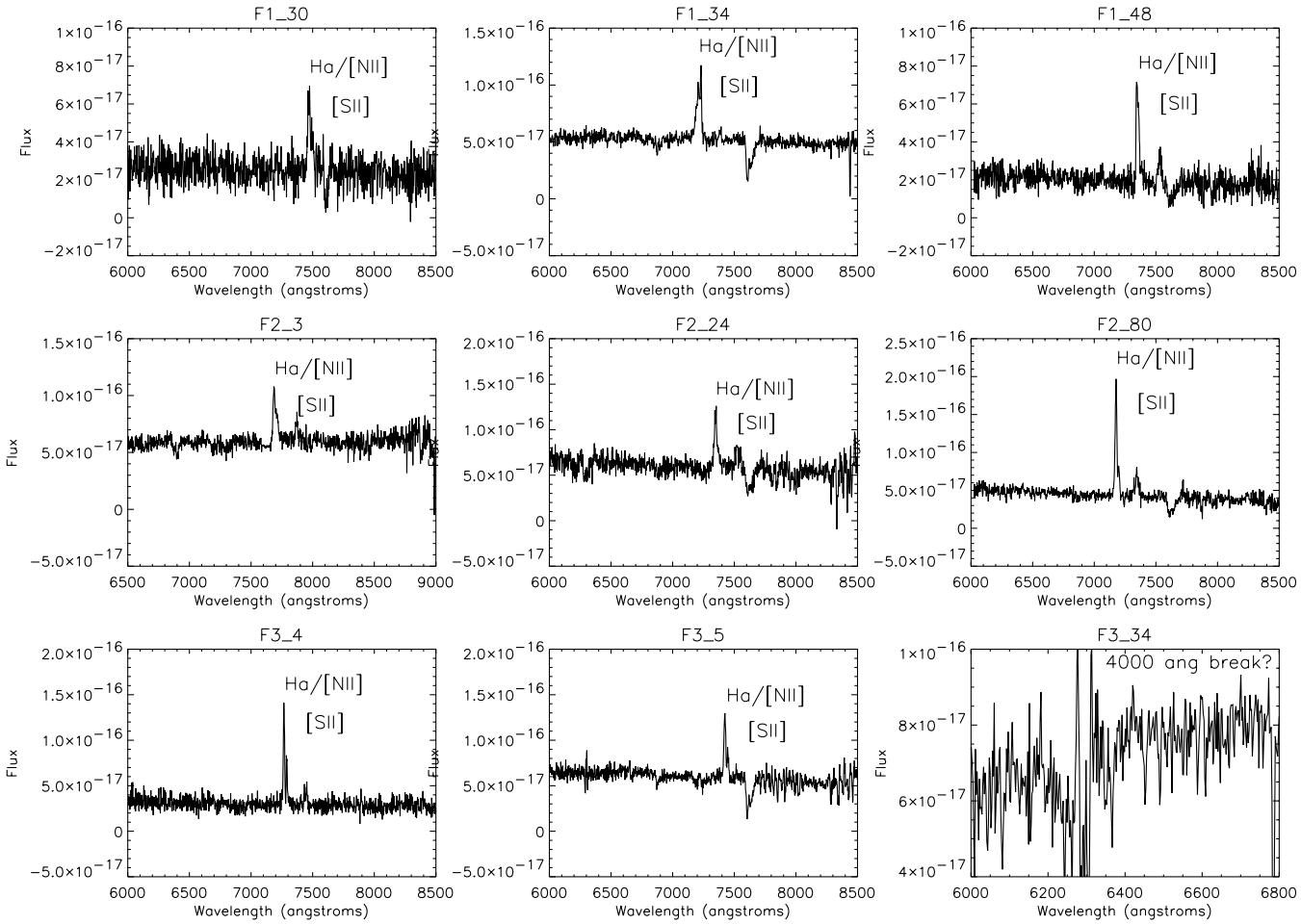

Figure 1 – *continued*

complete subsample of the 12-μm survey. We are complete to the 5σ flux limit of the survey, and to $R = 19.6$ mag for the optical identifications and redshift information. We can thus use the *accessible volume* method (Avni & Bahcall 1980) to determine the 12-μm luminosity function in this sample, whose 12-μm flux limit is a factor of > 20 deeper than existing determinations of the mid-IR luminosity function (Hacking et al. 1987). We use the standard $1/V_{\rm max}$ method to determine the luminosity function, with the volume determined from the maximum distance at which a source would be detected ie. the accessible volume. The luminosity function contribution of each object is $1/V_{\rm max}$ where $V_{\rm max}$ is given by the redshift at which an object would drop out of either the survey data or the follow-up programme, whichever is smaller.

Thus:

$$\Phi(L)\mathrm{d}L = \sum_i \frac{1}{V_i}, \tag{1}$$

where $\Phi(L)$ is the number of objects Mpc^{-1} in the luminosity range L to $L + \mathrm{d}L$ and

$$V_i = \min(V_{\mathrm{opt},i}, V_{12,i}), \tag{2}$$

where $V_{\mathrm{opt},i}$ is the volume in which the ith object could have been detected down to the $R = 19.6$ magnitude limit of the optical follow-up, and $V_{12,i}$ is the volume in which the ith object could have been detected down to the 500-μJy flux limit in the original survey. The volumes are calculated taking into account the variable flux depths of the original 12-μm survey (see Paper I).

The luminosity function produced from these considerations is shown in Fig. 4. As can be seen, the luminosity function is a fairly close match to existing 12-μm luminosity function determinations based on low-redshift *IRAS* data (see e.g.Fang et al 1998). The only substantial excursion from the local luminosity function occurs at the highest luminosities. As these high-luminosity bins are also dominated by the highest redshift objects, this might be taken as evidence for evolution. Combining the two highest luminosity bins to provide better statistics (three objects) at the highest luminosities suggests a $\sim 3\sigma$ significance difference between the current luminosity function and that derived from *IRAS* (Fang et al. 1998; Rush, Malkan & Spinoglio 1993). The mean redshift for objects in this bin is 0.7, implying density evolution at a rate of $(1 + z)^8$ or luminosity evolution at a rate of $(1 + z)^5$ with large uncertainties on these exponents. These values are broadly consistent with the evolution in the ultraluminous *IRAS* galaxies suggested by Kim & Sanders (1998) and with that suggested by Xu (2000) for the 15-μm population. However, as yet we have only a small number of objects at the highest luminosities. Indeed, the highest redshift bin contains only one object, F4_12. This is one of only two broad-line objects in the survey as well as being at the highest redshift, so it might be an unusual object that is biasing the statistics. There

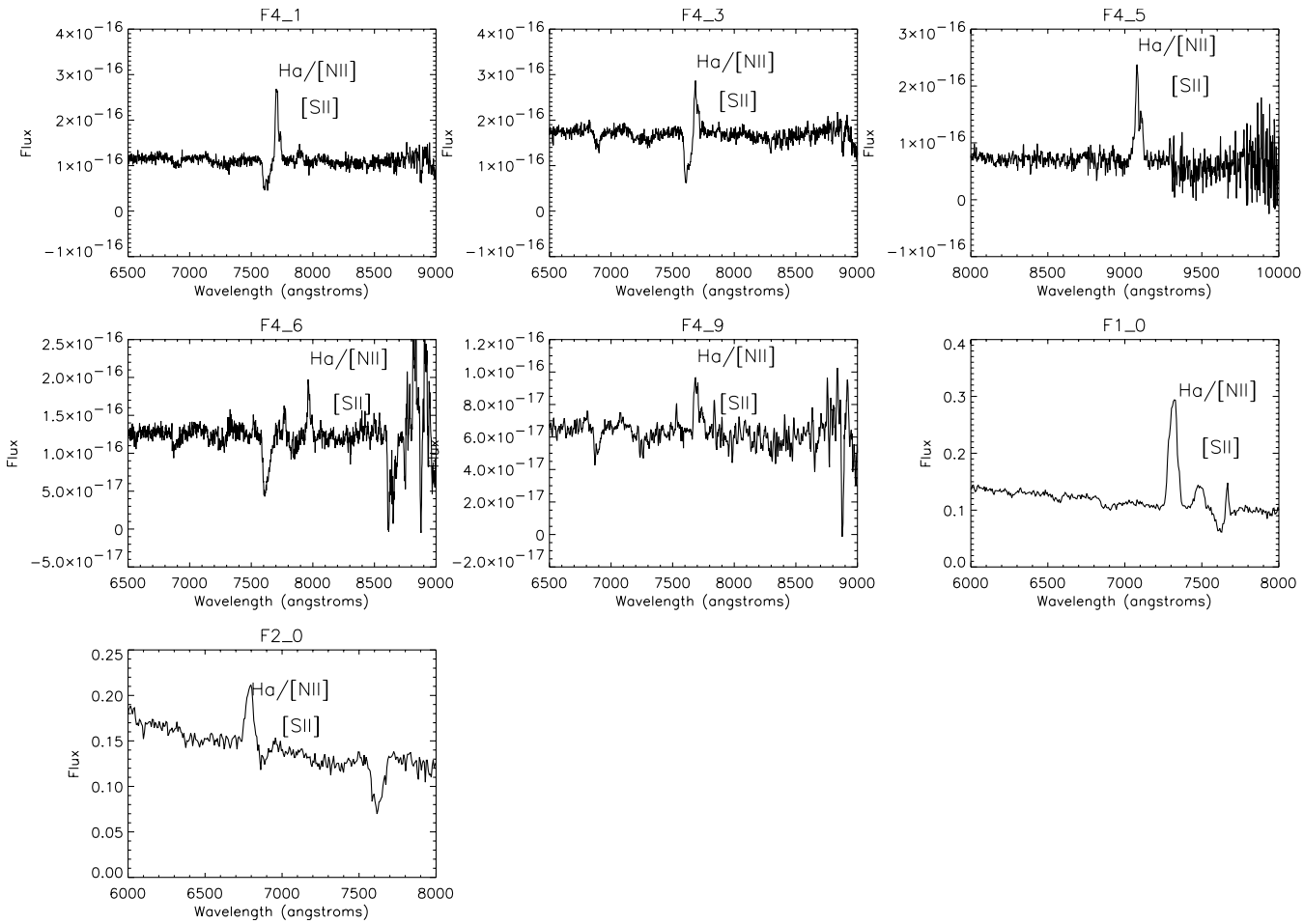

Figure 1 – *continued*

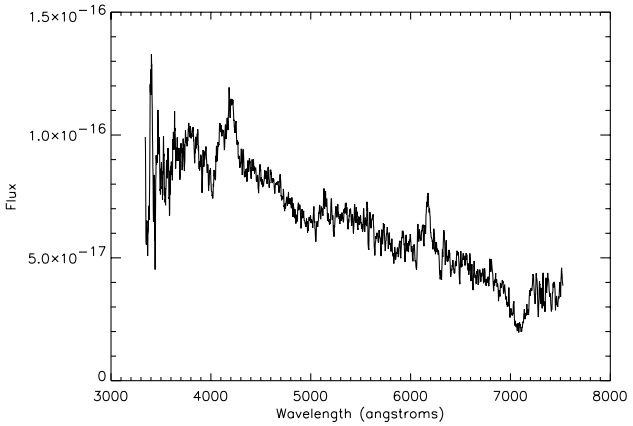

Figure 2. F4_12 spectrum: spectrum for the 12-μm selected quasar discovered in this survey.

may also be additional biases entering the data, e.g. Malmquist or Eddington biases, as the sample size is so small. These issues will be addressed when the identification programme is complete and we have a larger number of sources.

These hints at evolution in the high-luminosity/redshift end of the population can only be confirmed by determining redshifts for the rest of the sample. As the remaining galaxies are optically faint ($R > 19.6$), there is a strong possibility that substantially more high-redshift galaxies will be found, allowing a much better examination of the high-redshift and high-luminosity end of the luminosity function.

7 EMISSION LINE DIAGNOSTICS

The nature of the ionizing spectrum in a galaxy can be determined by examining emission-line ratios (Baldwin, Phillips & Terlevich 1981). Standard ratios include Hα/[N II] and Hα/[S II], which can be determined for most of the objects in the current sample, as well as [O I]/Hα, [O III]/Hβ and [O II]/Hβ. These latter ratios are not available for most of the objects in the sample since our spectral range did not extend far enough into the blue, or go deep enough to detect the weak [O I]6300 line. Consideration of the standard emission line diagnostic plots shows that we can attempt a classification using just the Hα, [N II] and [S II] lines we have for the majority of the objects. Our classification diagram is shown in Fig. 5. On this basis we find that the majority of our 12-μm sources (11/16 where appropriate data is available) have H II region-like spectra, i.e. are powered by starbursts, while 4/16 have Seyfert 2 (Sy2) like spectra, i.e. contain and may be powered by active nuclei. Two further objects have broad line Sy1-like spectra, producing a total of 6/18 objects that contain AGN. Three objects are not clearly classified by this technique and could be composite objects or LINERs.

We can extend this classification scheme for the four objects at

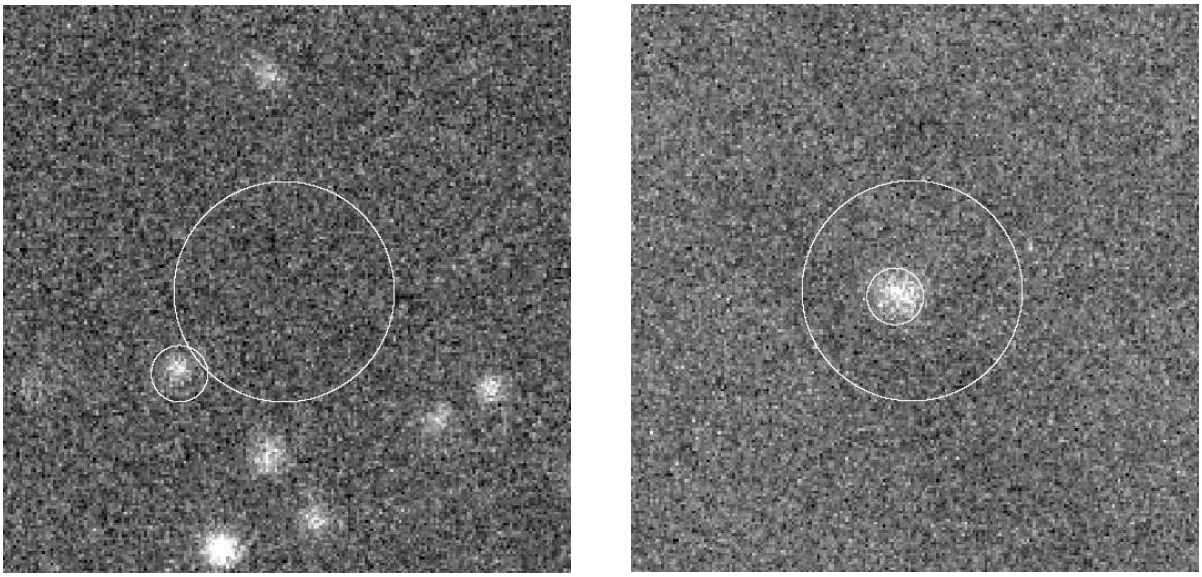

Figure 3. *R*-band images of 12-μm optical blank fields: F4_2 (left) and F4_11 (right). The images are 31.4 arcsec to a side. The nominal position of the *ISO* source is at the centre of each image. The astrometric accuracy of the *ISO* observations is 6 arcsec (2σ) (Paper I) and this is shown by the large circle. A smaller circle highlights the likely identification. The F4_2 identification has $R \sim 22$ F4_11 has $R \sim 20$. See text for details. Images are of similar depths reaching $R \sim 23$. The scaling is linear, so chosen to highlight relevant features.

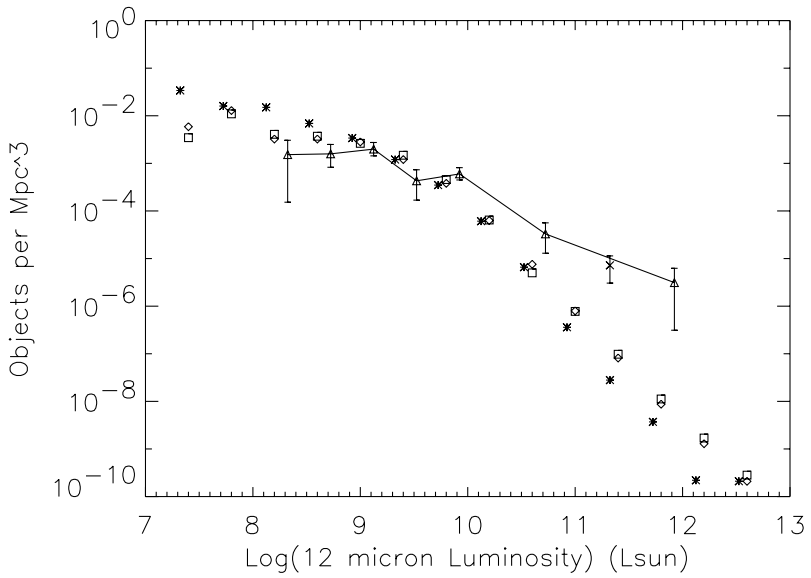

Figure 4. The 12μm luminosity function from Fang et al. (1998) (open squares and diamond for two different corrections to the local density field), Rush et al. (1995) stars, with luminosity divided by a factor of 1.5 to correct for photometric problems from the use of ADDSCAN data (Alexander & Aussel, private communication), and from the present work (triangles joined by a line). Note the similarities between the older, *IRAS* LF determination and the present, *ISO* determination, and the possible departure at high luminosities which equate to high redshifts. Also shown (X) are the last two bins of the new luminosity function combined to provide a better determination of the evolution at the highest redshifts.

high enough redshift and with sufficient signal-to-noise in their spectra to detect Hβ and [O III]. Of these objects only one is fully classified using just Hα, [N II] and [S II]. This object, F1_12, is classified as a Sy2 by both methods. Of the other three objects where we can use Hβ and [O III], F1_5 was previously unclassified as a result of poor [S II] detection, and the others, F1_11 and F4_5, have mixed classifications. Once Hβ and [O III] ratios are included, we find that F1_5 and F1_11 appear to be starbursts (ie. H II region-like). F4_5 appears to have a confused classification, with [O III]/Hβ versus [S II]/Hα indicating an H II region spectrum, and [O III]/Hβ versus [N II]/Hα indicating a Sy2 spectrum. On further examination it appears that the [S II] line strength may be underestimated because of a sky absorption feature at the extreme red part of the optical band (~9300 Å). We thus tentatively conclude that it is in fact a Sy2.

Thus the final tally is 14 starbursts, seven AGN (Sy1 and Sy2), one mixed and one unclassifiable. Of the objects where we have a firm classification, 1/3 (7/21) are AGN-type and 2/3 (14/21) are starbursts. We find no significant difference between 12-μm luminosities of the two classes, H II and Seyfert, though the most luminous objects are from the Seyfert class.

The Rush et al. (1993) sample of local 12-μm selected objects

had an AGN fraction of 13 per cent, so the larger fraction we have found here, 33 per cent, may represent some evolution in the population. Alternative explanations, such as different *K*-corrections between AGN and non-AGN containing objects, and greater prominence in the optical for AGN objects, are also possible. These possibilities will be investigated when the identification programme for the complete 12-μm survey is finished.

8 DISCUSSION

8.1 Physical associations

If we examine the redshift distribution, we find several clumps of objects that appear to group in redshift. These include an apparent group around $z = 0.11$ in Field 1, and around $z = 0.17$ in Field 4. We can test the reality or otherwise of these associations by examining the positions of the objects on the sky. In Field 1 we do indeed find that the objects F1_0, F1_7 and F1_9 appear to have a close physical association. They form a small group covering a region ∼1 arcmin across, corresponding to ∼100 kpc at $z = 0.11$, using our assumed cosmology (see Fig. 6). These objects may thus be part of a small group or weak cluster. One other object in Field 1 is at roughly the same redshift, F1_10 at $z = 0.113$. It is much further away on the sky, 7.5 arcmin, corresponding to 750 kpc. It might thus be part of some weak larger scale structure, but this is difficult to assess with the small numbers of redshifts we have. A simple analysis, using the luminosity function derived in Section 6, suggests that the association of F1_10 with the other three objects is only marginally significant, at ∼90 per cent level.

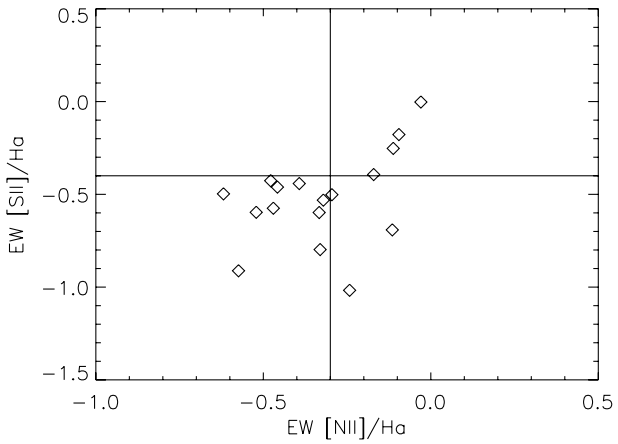

Figure 5. Emission line diagnostics. Starburst-type objects will lie in the lower left corner, AGNs in the upper right. Objects in the lower right corner receive a mixed classification, and may be composite objects or possibly LINERs. The broad line objects, F4_12 and F1_34, are not plotted on this diagram.

In Field 4 we find that F4_9 and F4_3 are close in both redshift (difference < 0.0005) and on the sky (39 arcsec), with a separation corresponding to 94 kpc at $z = 0.17$. They are thus likely to be a close pair of galaxies. F4_1, in contrast, is significantly further away in both redshift (0.004 in z) and angular separation (4.8 arcmin). It is thus unlikely that there is a strong physical association between F4_1 and the other two objects.

It is thus possible that five of our 12-μm sources appear in two groups, though better statistics are needed to determine if the correlation function of 12-μm selected objects is any different from optically selected, normal galaxies.

8.2 Bolometric luminosities

Spinoglio et al. (1995) found a correlation between 12-μm luminosity and bolometric luminosity. The basis for this correlation was argued to be that the wavelength is a 'pivot point' between the optical emission, which rises more slowly than linearly with bolometric luminosity, and the mid- to far-IR, which rises more rapidly than linearly with bolometric luminosity. They also found that the constant of proportionality relating 12-μm and

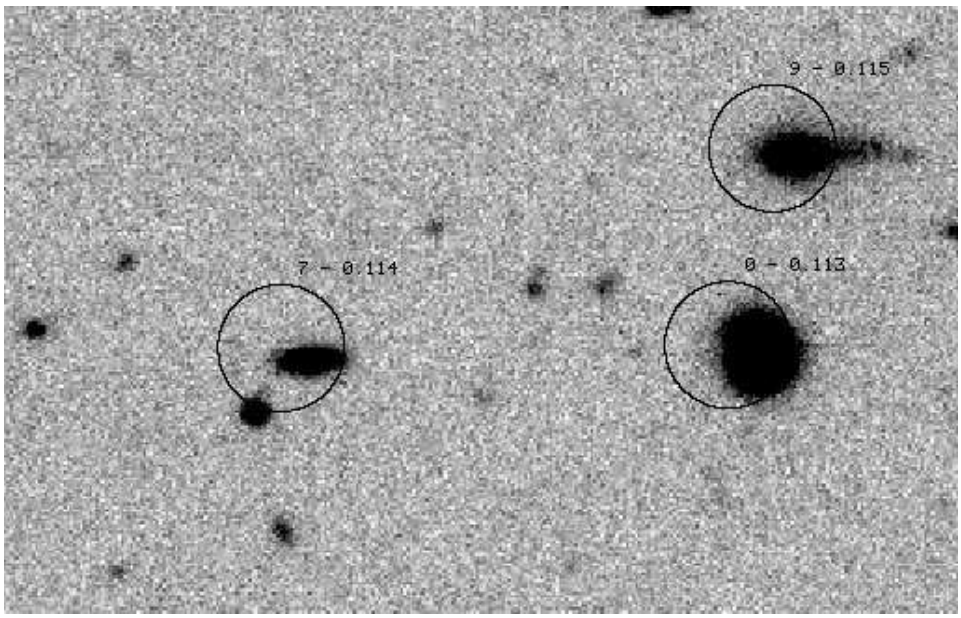

Figure 6. Group of objects in Field 1. Circles show the 6-arcsecond 2σ astrometric errors on the *ISO* source position. Text indicates the number of the source in the Field 1 list and its redshift. The image is 100 by 66 arcsec. Note also the disturbed morphology of source F1_9. North is up and east is to the left. Scaling is linear, and chosen to highlight relevant features.

bolometric luminosity is different for starburst and AGN sources – thus $L_{\rm bol} = 14L_{12}$ for starbursts and $L_{\rm bol} = 5L_{12}$ for AGNe, where $L_{12} = \nu(12\mu{\rm m})L_{\nu}(12\mu{\rm m})$ in solar units. If we assume that our optical classifications of these objects genuinely identify the source of their luminosity, then we can calculate the bolometric luminosity of the sources. These are given in Table 2. We find that the typical bolometric luminosity for our 12-μm sources is around $10^{10.5}\,{\rm L}_{\odot}$. The population of mid-IR sources so far uncovered would thus appear to have relatively moderate luminosities, and to not represent any substantial new population of dust-enshrouded starbursts or AGN. Our highest luminosity source, F4_12, however, turns out to have a bolometric luminosity of $10^{12.7}\,{\rm L}_{\odot}$, approaching that of hyperluminous infrared galaxies. Since this is the highest redshift object in the sample, and our luminosity function analysis seems to indicate strong evolution at high redshifts or high luminosities, then one can speculate that this might be the first member of a lurking population of obscured high-luminosity systems that we have yet to uncover. Completion of our identification programme can test this idea.

8.3 The nature and evolution of the 12-μm milliJansky population

Low-luminosity 12-μm selected sources appear to be similar to the local samples. We find that about 1/3 of them contain AGNe while the remainder are powered by starbursts. These fractions are somewhat higher than those discussed by Rush et al. (1993). At the highest luminosities there are hints of strong evolution being detected, but these are currently dominated by small number statistics. With deeper observations we will not only be able to confirm the presence of evolution but also test claims, based upon the 15-μm surveys, that a substantial new population of objects becomes significant at the ∼1-mJy flux level (e.g. Elbaz et al. 1998; Aussel et al. 1999). It should be noted that selection of objects at 12 μm is much less affected by *K*-corrections caused by the complex mid-IR spectral energy distributions of star-forming galaxies and AGN (Xu et al. 1998) than selection at 15 μm. It has been suggested (Xu 2000) that the bump in 15-μm number counts at ∼0.4 mJy is entirely caused by this *K*-correction effect and not by any new population. While the current survey is working at somewhat brighter fluxes, we find no clear evidence for such a population. However, if such sources are optically faint, whether intrinsically or as a result of their redshift, they may well have been missed by the optical selection criterion. Completion of the optical identifications and redshift measurements for all the objects in the survey is needed to test these claims and is thus a high priority.

8.4 Future prospects

The present paper is only the first step in following up the galaxies found in this 12-μm *ISO* survey. We have here discussed the results of redshift measurements on 26 of the 36 galaxies with fluxes above the 5σ flux limit of our survey, forming a complete subsample with $R < 19.6$. While we are able to obtain interesting conclusions, they are clearly limited by small number statistics, and we are as yet unable to study objects with a large $F_{12}/F_{\rm opt}$ ratio (e.g. F4_2 which has F_{12} of 3.6 mJy, but an *R* magnitude of ∼22). Completing the redshift observations for the $10 > 5\sigma$ sources so far unobserved is clearly a high priority. In Field 1, where we have deeper optical data, nearly all of the 12-μm sources are identified with objects brighter than $R = 23.2$. If this is representative of the rest of the sample, then complete identifications and spectroscopy should be fairly easy to obtain. Perhaps more interesting is the prospect of extending our redshift observations to fainter 12-μm fluxes. If we go to a 4σ detection limit, rather than 5σ, we would include ∼45 more sources. All of these objects, again, are detected in our deep optical observations of Field 1, so such a study is eminently feasible, given deeper optical imaging and a moderate amount of time for spectroscopy. We will thus be able to substantially increase the number of redshifts we have for faint 12-μm sources, and will be able to place the tentative conclusions of the present paper on a much firmer footing. Such observations will make an excellent parallel study to the 15-μm surveys also underway (e.g. Oliver et al. 2000; Elbaz et al. 1999).

9 CONCLUSIONS

We have obtained spectroscopy for a complete $R < 19.6$ subsample of our 12-μm survey with the *ISO* satellite. The redshifts of these objects range from 0.032 to 1.2, with derived bolometric luminosities ranging from $10^{9.3}$ to $10^{12.7}\,{\rm L}_{\odot}$. There is tentative evidence for strong evolution at the high-luminosity and/or high-redshift end of the luminosity function. We find that 1/3 of these sources contain an AGN, while the rest seem to be powered by starbursts. At this stage our conclusions are limited by small number statistics, but there are very good prospects for extending the identification programme for this survey, and thereby allowing stronger, more definitive conclusions to be drawn.

ACKNOWLEDGMENTS

This paper is based in part on observations carried out at the European Southern Observatory, La Silla, Chile, and in part on observations with *ISO*, an ESA project with instruments funded by ESA Member States (especially the PI countries: France, Germany, the Netherlands and the United Kingdom) and with the participation of ISAS and NASA. It is a pleasure to thank Scott Croom and Steve Warren for the provision of the INT Wide Field Survey optical data for Field 1, and the UKIRT minisurvey team for providing similar infrared data. The Digitised Sky Survey was produced at the STSCI under US Government Grant NAG W–2166. This research has made use of the NASA/IPAC Extragalactic Database (NED) which is operated by the Jet Propulsion Laboratory, California Institute of Technology, under contract with the National Aeronautics and Space Administration. The USNO-A survey was of considerable help, and we would like to express our thanks to all those who helped to produce it. We also thank Herve Aussel, Dave Alexander and Matt Malkan for useful discussions. DLC acknowledges support from a PPARC post-doctoral position and, during the early stages of this work, an EU TMR Network post (FMRX-CT96-0068). We also thank the anonymous referee for many useful comments.

REFERENCES

Avni Y., Bahcall J. N., 1980, ApJ, 235, 694
Almaini O., Lawrence A., Boyle B. J., 1999, MNRAS, 305, L59
Aussel H., Elbaz D., Cesarsky C., Stark J-L., 1999, in Cox P., Kessler M., eds, The Universe as seen by *ISO*. ESA Publications Division, Noordwijk, p. 427
Baldwin J. A., Phillips M. M., Terlevich R., 1981, PASP, 93, 5
Cesarsky C. J. et al., 1996, A&A, 315, L32
Clements D. L., Sutherland W. J., Saunders W., McMahon R. G., Maddox S., Efstathiou G. P., Rowan-Robinson M., 1996, MNRAS, 279, 459

Clements D. L., Desert F-X., Franceschini A., Reach W. T., Baker A. C., Davies J. K., Cesarsky C., 1999, A&A, 346, 383 (Paper I)
Eales S., 1999, ApJ, 515, 598
Elbaz D. et al., 1998, in Smith E. P., Long K. S., eds, ASP Conf. Ser. Vol. 207, The Next Generation Space Telescope: Science and Technology Colloquium. Aston. Soc. Pac., San Francisco, p. 47
Elbaz D. et al., 1999, A&A, 351, L37
Fang F., Shupe D. L., Xu C., Hacking P. B., 1998, ApJ, 500, 693
Gispert R., Lagache G., Puget J-L. ., 2000, A&A, 360, 1
Haas M., Klaas U., Couldson I., Thommes E., Xu C., 2000, A&A, 356, L83
Hacking P., Houck J. R., Condon J. J., 1987, ApJ, 316, L15
Hughes D. H., Lowenthal J., 2000, Proc. UMASS/INAOE Conf., Deep Submillimetre Surveys. World Scientific Press, Singapore, in press
Kawara K. et al., 1998, A&A, 336, L9
Kessler M. et al., 1996, A&A, 315, L27
Kim D-C., Sanders D. B., 1998, ApJS, 119, 41
McMahon R. G., Walton N. A., Irwin M. J., Lewis J. R., Bunclark P. S., Jones D. H. P., Sharp R. G., 2000, New Astron., in press
Mirabel I. F. et al., 1998, A&A, 333, L1
Oliver S. et al., 2000, MNRAS, 316, 749
Osterbrock D. E., , Astrophysics of Gaseous Nebulae and Active Galactic Nuclei. University Science Books, Mill Valley
Patat F., 1999, The EFOSC 2 User's Manual. ESO Publications Division, Garching
Puget J-L. et al., 1996, A&A, 308, L5
Puget J-L. et al., 1999, A&A, 345, 29
Rush B., Malkan M., Spinoglio L., 1993, ApJS, 89, 1
Sanders D. B., Mirabel I. F., 1996, ARA&A, 34, 749
Serjeant S. B. G. et al., 1997, MNRAS, 289, 457
Serjeant S. B. G. et al., 2000, MNRAS, 316, 768
Spinoglio L., Malkan M., Rush B., Carrasco L., Recillas-Cruz E., 1995, ApJ, 453, 616
Xu C. et al., 1998, ApJ, 508, 576
Xu C., 2000, pre-print (astro-ph/0004216)

This paper has been typeset from a TEX/LATEX file prepared by the author.